



FACILE SYNTHESIS STRUCTURAL CHARACTERIZATION PHOTOCATALYTIC AND ELECTROCHEMICAL APPLICATIONS OF $\text{CrO}_4\text{-CeO}_2$ NANOCOMPOSITE MATERIAL

K. Subashri

*Ph.D Research Scholar, Department of Chemistry, Centre for Research and Evaluation, Bharathiar University,
Coimbatore 641046, Tamilnadu, India.*

ABSTRACT

The CeO_2 and $\text{CrO}_4\text{-CeO}_2$ nanocomposite material prepared by co-precipitation method and sonication technique and nanocomposite material characterized by HR-SEM and HR-TEM result demonstrate that the initial spherical shape like an irregular particle for the nanocomposite material. The EDX analysis confirms that Cr, Ce and O are present from nano photocatalyst. The X-ray XRD study catalyst are fine crystallized among that little surface areas and to gives high crystalline size by HR-TEM images, The PL measured low intensity and UV-Vis DRS calculated low band gap energy also result as conformed high photocatalytic activity on by Trypan Blue (TB) dye at $\text{CrO}_4\text{-CeO}_2$ nanocomposite material. The prepared $\text{CrO}_4\text{-CeO}_2$ nanocomposite material high efficiency of photocatalyst that of CeO_2 under UV and solar-light irradiation and mechanism has been discussed and high current produced from DSSCS application of, electrochemical industrial was done; prepared nanocomposite material was stability and reusability of photocatalyst.

1. INTRODUCTION

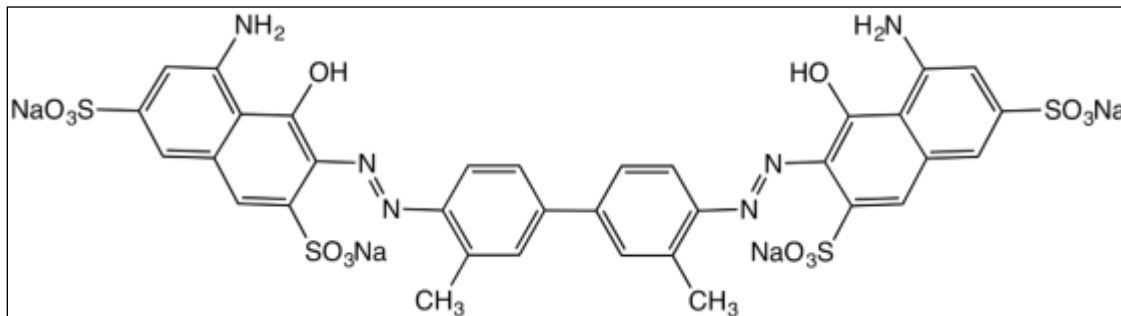
Cerium dioxide is an important rare earth oxide, which has multiple applications such as electrolyte material of solid oxide ultraviolet blocking materials, catalysts, chemical mechanical polishing, and oxygen gas sensors [1]. The photostability of pigments can be enhanced by the addition of cerium. CeO_2 nanoparticles are interesting due to their wide variety of applications in polishing agents, sunscreens, solid electrolytes, solar cells, fuel cells, phosphorescent/luminescent materials, photocatalysis, sensors, oxygen pumps, and metallurgy [2]. Nanostructured cerium oxide powders can effectively degrade pollutants. CeO_2 nanostructure is an n-type semiconductor that is coupled with wealthy oxygen vacancies, in current research, ceria has been established to be a capable photocatalyst for the removal of industrial pollutants in the environment owing to the redox property of the two stable oxidation states of ceria ($\text{Ce}^{4+}/\text{Ce}^{3+}$), strong absorption of light, stability, non-toxicity, and availability [3-6].

In this work we report on a study in prepared nanocomposite material was characterized by HR-SEM with X-ray (EDX) analysis, HR-TEM, XRD analysis, PL analysis and UV-Vis DRS analysis. $\text{CrO}_4\text{-CeO}_2$ nanocomposite material will expand the photocatalytic application of UV-light and Solar-Light irradiation at 60 min and electrochemical application from synthetic dye based DSSCS analysis result was obtained.

2. EXPERIMENTAL SECTION

2.1. Materials

The Ammonium cerium (IV) Sulfate, Trypan Blue (TB), $(\text{NH}_4)_2\text{Cr}_2\text{O}_7 \cdot 2\text{H}_2\text{O}$, Citric acid, ammonia and ethanol solution and Fluorine doped Tin oxide FTO-plate) and Ruthenium dye (535-bisTBA, N719) solution, it was Sigma Aldrich reagent and was used as such All glassware was cleaned with acid and washed thoroughly with distilled water. Water is used as an experiment throughout. The Trypan Blue (TB) Chemical structure shown in Fig. 1.



2.2. Synthesis of CrO₄-CeO₂ nanocomposite material

(NH₄)₂Cr₂O₇·2H₂O were first dissolved with distilled water respectively, The resulting solution was added dropwise into Ammonium cerium (IV) sulfate with ammonia solution added in 1:2 ratio. Solution with anhydrous ethanol as solvent at room temperature under vigorous stirring 4 h until precipitate formed was placed in sonication 20 min. The obtained precipitate was filtered and washed with distilled water and ethanol until alkali phases were removed from precipitation. Then the precipitate was collected and dried in oven at overnight. The resulting powder was finally calcined at 150, 300 and 450 °C for 3 h. The prepared CrO₄-CeO₂ 450 °C heat treatment at a higher photocatalytic activity.

2.3. Characterization of CrO₄-CeO₂ Nanocomposite Material

Ultraviolet and visible (UV-vis) absorbance spectra were measured over a range of 800–200 nm with a Shimadzu UV-1650PC recording spectrometer using a quartz cell with 10 mm of optical path length. High resolution Scanning Electron Microscopy (HR-SEM) as well as Elementary Dispersive X-ray (EDX) evaluation experiments were performed on a FEI Quanta FEG 200 instrument with EDX analyzer facility at 25 °C. The nanoparticles size and structure verifications were done by Transmission Electron Micro-scopy (HR-TEM) making use of PHILIPS CM200. Each spectrum was recorded with an acquisition time of 18 s. XRD spectrum was recorded on the X'PERT PRO model X-ray diffractometer from Pan Analytical instruments operated at a voltage of 40 kV and also a current of 30 mA with Cu K α radiation. Photoluminescence (PL) spectra at a room temperature were recorded using a Perkin-Elmer LS 55 fluorescence spectrometer. UV spectral measurements were done using a Hitachi-U-2001 spectrometer. Ultraviolet and visible (UV-vis) absorbance spectra were measured over a range of 800–200 nm with a Shimadzu UV-1650PC recording spectrometer using a quartz cell with 10 mm of optical path length. The antibacterial activity was studied by disc diffusion method; the test compound was dissolved in DMSO (200 mg/mL) for about half an hour. Commercially available drug disc, Ciprofloxacin (10 mg/ disc) was used as positive reference standard and Cyclic voltammetry (CV) measurements were carried out using CHI 60 AC electro-chemical analyzer (CHI Instruments Inc. USA).

2.4. Photocatalysis

The photocatalytic activities of CrO₄-CeO₂ nanocomposite material were evaluated by the photodegradation of dye. The light irradiation at 365 nm. The reaction was carried out at ambient temperature (303 K). The experiment, aqueous suspensions of dye (40 mL, 1 × 10⁻⁴ M) and 0.080 g of photocatalyst were loaded in reaction tube of 50 mL capacity with a Prior 60 min in the irradiation, the suspension was magnetically stirred in dark to ensure the establishment of an adsorption or desorption equilibrium. The suspension was kept under constant air-equilibrated condition. At the intervals of given irradiation time. The suspension was measured spectrophotometrically within the theory to Beer-Lambert law limit.

3. RESULTS AND DISCUSSION

3.1. High-Resolution Scanning Electron Microscope Analysis (HR-SEM) & Energy Dispersive Analysis (EDX).

The scanning electron microscope (SEM) is a technique for high-resolution surface imaging. The texture and morphology of the catalyst are critical parameters that influence photocatalytic activity. **Figures 3.1.a-c** show a close-up and overall view of the sample. The product has a uniform homogeneous dispersal spherical structure with cluster formation. The diameter of these particles is approximately 10 nm, as shown in **Fig.3.1.a**. Kumar et al [7] synthesized cerium oxide nanoparticles with a 20 nm size that have a uniform homogeneous dispersal spherical structure, good thermal stability, and good photocatalytic activity. The elemental composition of a synthesized CrO₄-CeO₂ nanocomposite material was evaluated using EDS. The EDS analysis reveals well-defined peaks of Cr, O, and Ce atoms, indicating that CrO₄⁻ has been incorporated with CeO₂, as shown in **Figure.3.1**

3.2. High-Resolution Transmission Electron Microscope Analysis (HRTEM)

A TEM uses energetic electrons to provide morphological, compositional, and crystallographic information on samples. TEM images were used to examine the surface morphology of prepared $\text{CrO}_4\text{-CeO}_2$. As shown in **Fig. 3.2.a**, the sample has spherical shapes with agglomeration and the diameter of the nano particles is about 100 nm. The prepared $\text{CrO}_4\text{-CeO}_2$ nanocomposite material has a spherical surface morphology. Hailstone et al [8] synthesized cerium oxide nanoparticles with 20 nm size that have a spherical shape like an irregular particle, good photocatalytic activity, and antimicrobial activity. The values obtained in this study agree well with those reported by another research group [9].

The prepared $\text{CrO}_4\text{-CeO}_2$ nanocomposite material has a morphological structure that resembles a spherical shape with irregular particles measuring 100 nm in size. At 100 nm magnifications, **Figure 3.2.b** shows the well-resolved lattice fringes. The average particle size distribution is depicted in **Figure 3.2.c**. The highlighted selected particle size at 0.456 nm is shown in **Figure 3.2.d**. The particle size observed in TEM studies agrees well with the average size obtained from XRD results. Using the "Image J Viewer" software skills, the image profile and normal particle range distribution were determined.

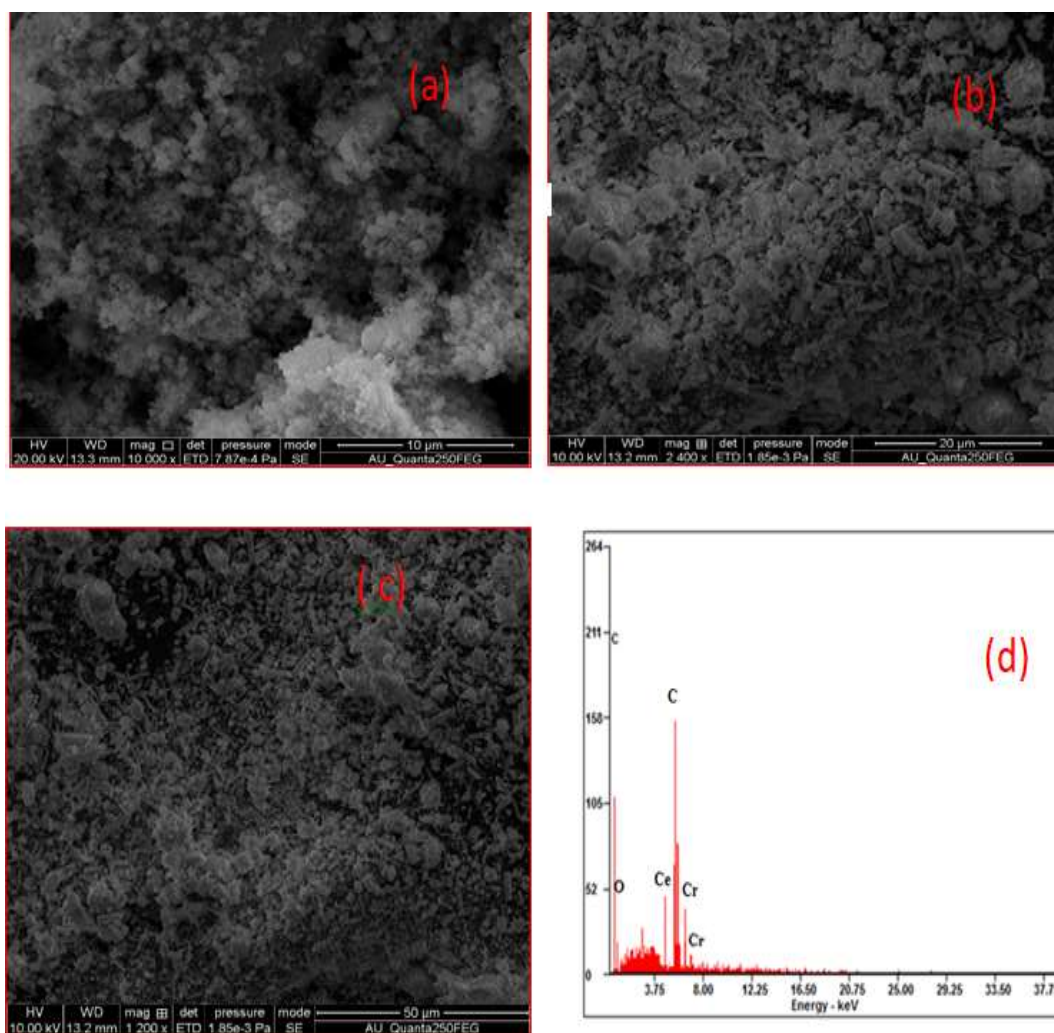


Figure.3.1. HR SEM image and EDX analysis of $\text{CrO}_4\text{-CeO}_2$ nanocomposite material

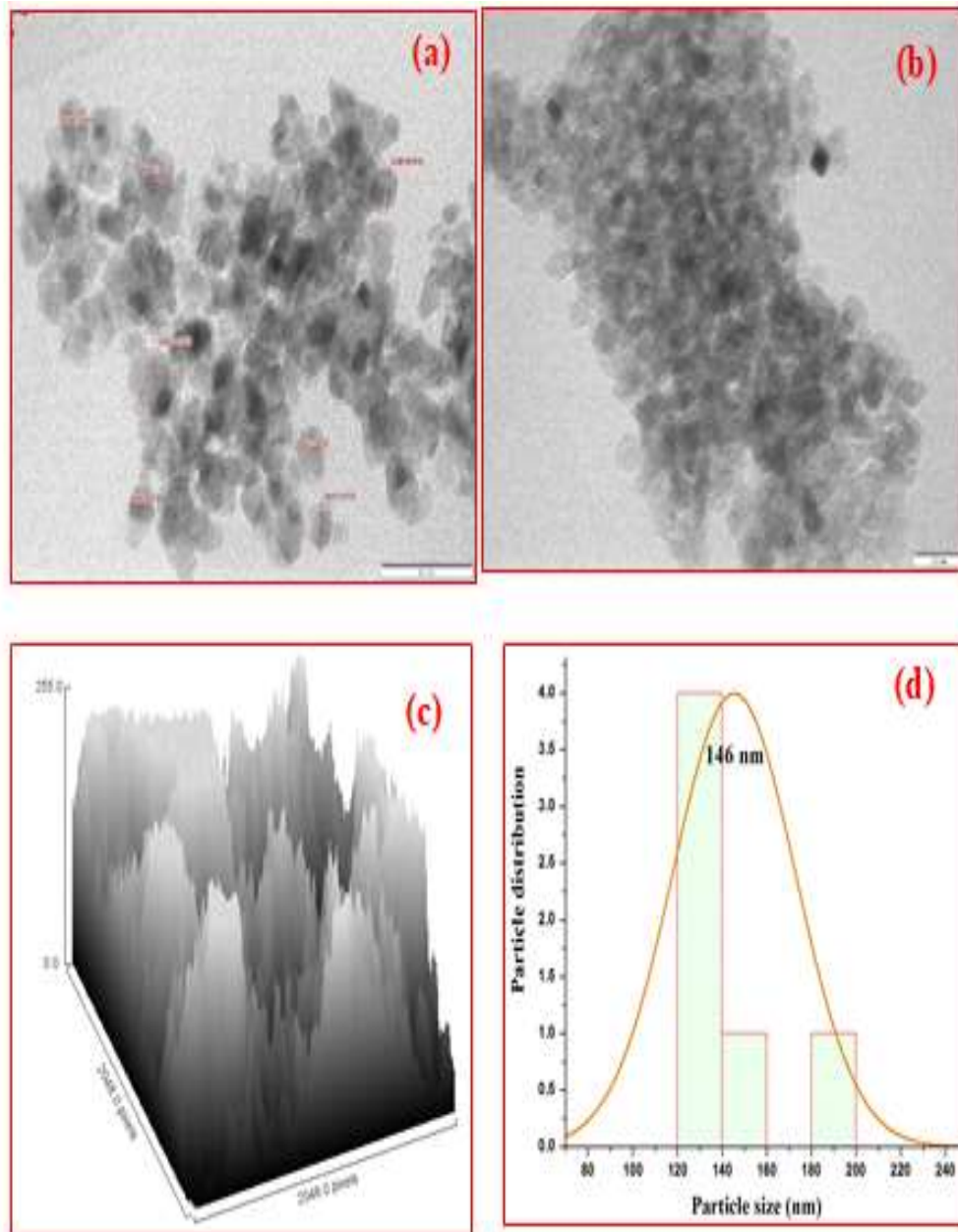


Figure.3.2. HR-TEM analysis of $\text{CrO}_4\text{-CeO}_2$ nanocomposite material (a,b) Image $\text{CrO}_4\text{-CeO}_2$ nanocomposite material (c) Surface plot and (d) particle size in selected area highlighted fig (a)

3.3 X-ray Diffraction (XRD)

The powder XRD study was carried out to find out crystalline structure of prepared $\text{CrO}_4\text{-CeO}_2$ nanocomposite material. The **Figures 3.3 a and b** displayed the XRD patterns of bare CeO_2 and prepared $\text{CrO}_4\text{-CeO}_2$ nanocomposite material. The XRD patterns of CeO_2 and prepared $\text{CrO}_4\text{-CeO}_2$ showed distinct peaks in the spectrum, the 2θ values at 28.53° , 33.09° , 47.50° , 56.26° , 59.13° , and 76.56° representing (111), (200), (220), (311), (322) and (311) planes respectively. As indexed in the Figure, all the diffraction patterns indicate the cubic phase (File No 34-0394 of the JCPDS). Thammadihalli et al [10] synthesized CeO_2 nanoparticles with have cubic phase and particle with 35nm size. The peak of the graph is in good agreement with the literature report.

In the XRD patterns of the prepared $\text{CrO}_4\text{-CeO}_2$ another sharp peak were observed for high crystalline nature by CrO_4 loaded CeO_2 . The peak intensity is lower, confirming the loading of $\text{CrO}_4\text{-CeO}_2$. Debye Schorr's equation was used to calculate the crystalline size of CeO_2 and prepared $\text{CrO}_4\text{-CeO}_2$. The Debye-Scherrer formula is used to calculate the average crystallite size of a nanocomposite material.

$$D = K\lambda / \beta \cos \Theta$$

Where, D = crystalline size of the nanocomposite material

K = shape factor (or) Dimensionless constant

λ = Wavelength of the X-rays

β = the full line width at the half-maximum elevation of the main intensity peak (FWHM), and

Θ = Bragg diffraction angle. Since this equation,

The crystalline size of CeO_2 nanocomposite material and prepared $\text{CrO}_4\text{-CeO}_2$ nanocomposite material are calculated about 29 nm and 23.2 nm correspondingly.

3.4 Photoluminescence Discharge Spectral Analysis (PL)

The electronic structure, transfer behavior, and recombination rate of photo excited electron-hole pairs in semiconductor materials can all be studied using photoluminescence spectroscopy (PL). Irradiative recombination of photo excited electrons and holes produces the PL spectra.

These charge carriers are crucial in determining the efficiency of photocatalytic activity. **Figures 3.4. a and b** depict the PL spectrum of CeO_2 and a prepared $\text{CrO}_4\text{-CeO}_2$ nanocomposite material with excitation wavelengths of 210 and 523 nm, respectively. It is primarily composed of two emission bands: a strong blue emission band at 210 nm and a green emission band at 523 nm. R.C Deus et al [11] reported a blue band at approximately 240 nm, as well as a green band at 529 nm. These values agree with the above result.

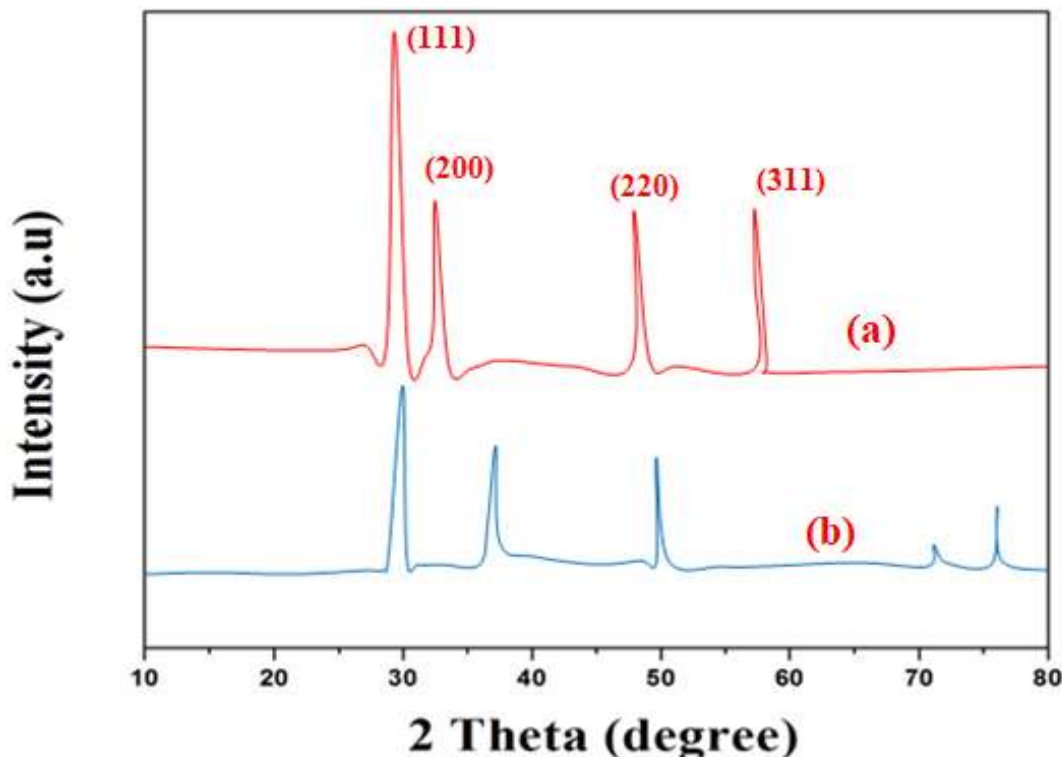


Figure.3.3. XRD pattern of (a) CeO_2 and (b) $\text{CrO}_4\text{-CeO}_2$ nanocomposite material

The recombination of electron-hole pairs in the nanocomposite material causes photoluminescence. The prepared $\text{CrO}_4\text{-CeO}_2$ has a lower PL intensity than CeO_2 . As a result, CeO_2 bands can be associated with bulk energy levels and high-intensity peaks. This matches their explanation for charge transfer (CT) transitions between O_2 and Ce^{4+} [6]. The peak intensity of prepared $\text{CrO}_4\text{-CeO}_2$ is low. The

characteristic photoluminescence peaks in the UV band are observed as a result of direct recombination of electrons in the Ce 4f conduction band with holes in the Oxygen 2p valence band, whereas the broad visible emission band has been proposed as a result of the presence of many point defects, such as oxygen vacancies, and suppression of recombination of the photogenerated electron-hole pairs by the CrO₄- loaded CeO₂. This catalyst becomes more photoactive when electron-hole recombination is inhibited [12,13].

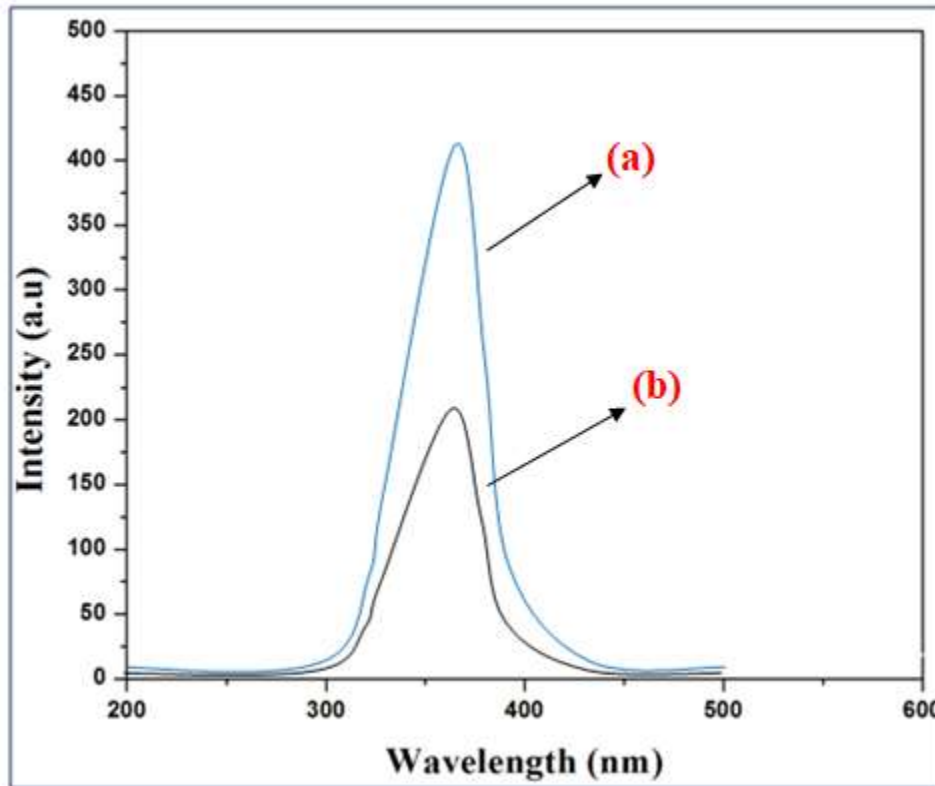


Figure. 3.4. PL analysis of (a) CeO₂ and (b) CrO₄-CeO₂ nanocomposite material

3.5 Diffuse Reflectance Spectroscopy

The UV-Vis DRS analysis is one of the spectra analysis show cut-off regions in a specific wavelength range which can be attributed to the photo-excitation of electrons from the valence band to the conduction band. The UV-Vis can be approximately calculated from the optical reflectance data by the Kubelka–Munk function,

$$A = F(R) = \frac{((1-R)^2)}{2R} \quad \dots (1.1)$$

where α is the absorbance coefficient, R is the diffuse reflectance (Guoli et al 2009).

An extrapolation of the linear region of a plot of $(F(R) hv)^2$ vs hv gives the value of the optical bandgap energy. The bandgap energy for nanocomposite material is calculated from $E = hv = hc/\lambda$. The bandgap energy of CeO₂ and the prepared CrO₄-CeO₂ nanocomposite material is 3.19 and 3.0 eV correspondingly show in Figures 3.5 a and b. These results showing prepared CrO₄-CeO₂ nanocomposite material low bandgap energy high photocatalyst and electrochemical applications were obtained [14-17].

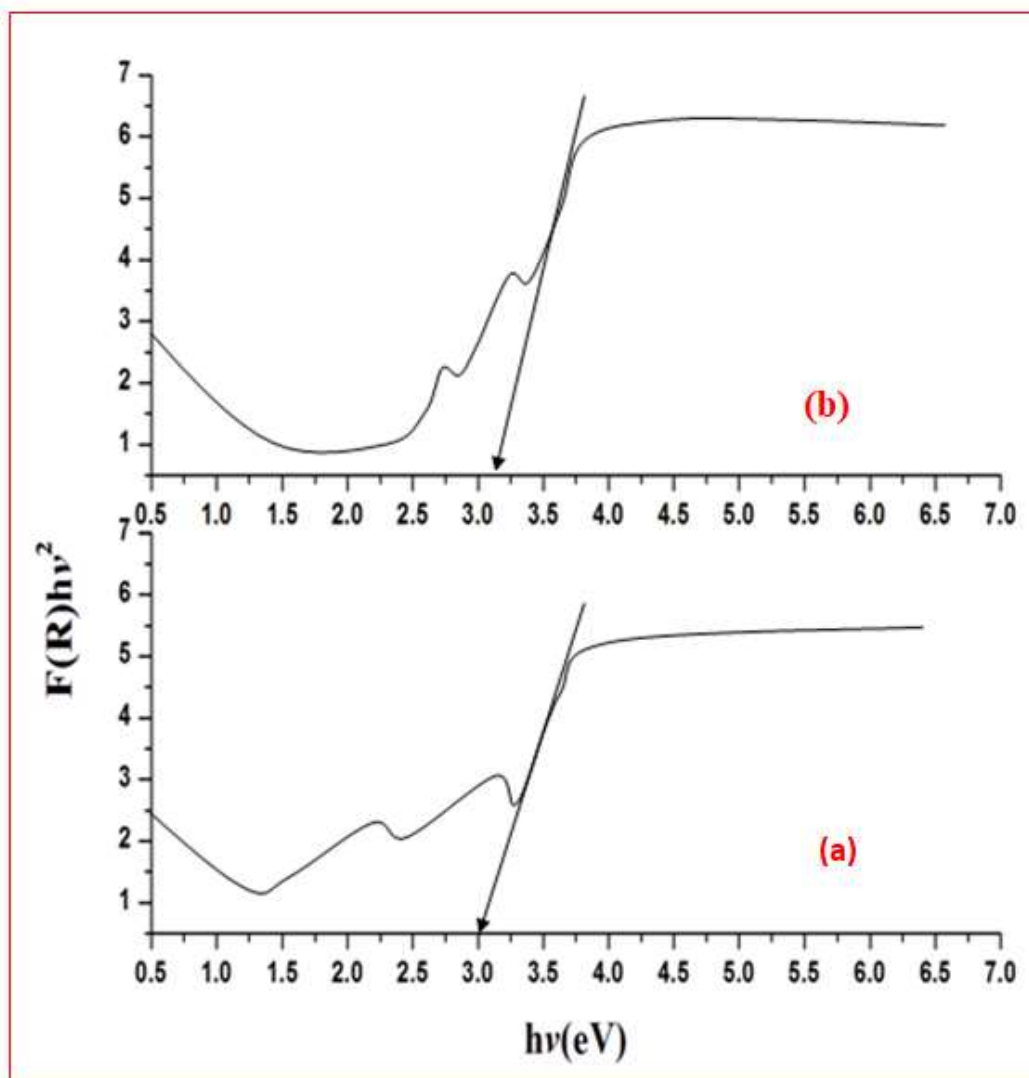


Figure. 3.5. UV-Vis DRS analysis of (a) CeO_2 and (b) $\text{CrO}_4\text{-CeO}_2$ nanocomposite material

3.6 Photocatalytic application under UV and solar-light

3.6.1 Primary Analysis

Figures 3.6.1. A and B show the photo degradability of Trypan Blue (TB) with various photocatalysts under UV and solar light. In the absence of UV and solar light, the percentage of dye degradation with $\text{CrO}_4\text{-CeO}_2$ is very low (curve-a). This could be due to dye adsorption on the catalyst's surface. The curve-b depicts the degradation of dye in the absence of a photocatalyst under UV and solar light. Self-photolysis is not a problem for dye. These findings suggest that both UV and solar light are required for the effective degradation of Trypan Blue (TB) dye. Under UV and solar light, the percentages of dye degradation with CeO_2 are 35% and 43%, respectively (curve-c). Under UV and solar light, the percentage of dye degradation with prepared $\text{CrO}_4\text{-CeO}_2$ is 80% and 85% (curve-d), respectively. This demonstrates that prepared $\text{CrO}_4\text{-CeO}_2$ degrades Trypan Blue (TB) more efficiently under solar light.

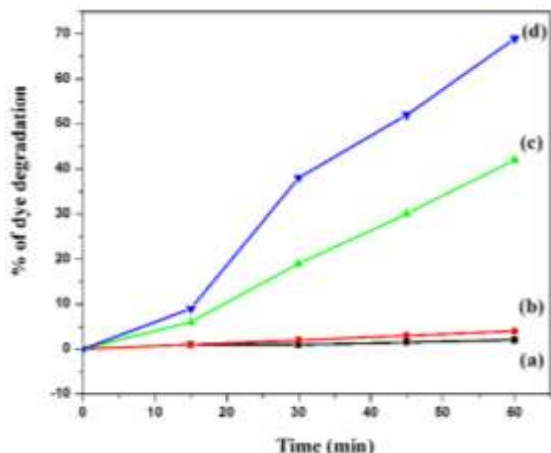


Figure 3.6.1. (A) Photodegradation study of TB dye under UV irradiation by (a) Dark (b) Nil catalysis (c) CeO₂ and (e) CrO₄- CeO₂ nanocomposite material

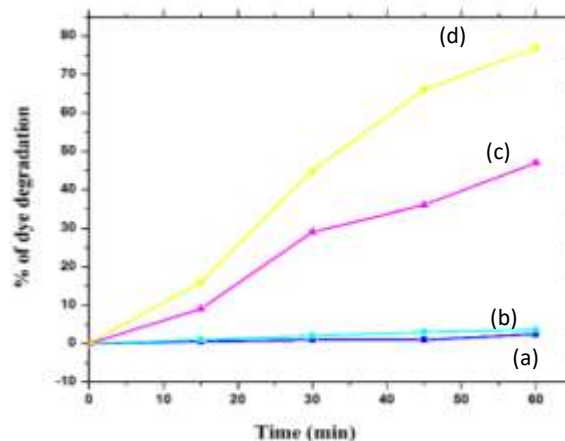


Figure 3.6.1. (B) Photodegradation study of TB dye under solar-Light irradiation by (a) Dark (b) Nil catalysis (c) CeO₂ and (e) CrO₄- CeO₂ nanocomposite material

➤ TB dye 1×10^{-4} , nanocomposite material suspended = 2 gL^{-1} , airflow rate 8.1 mL s^{-1} , IUUV = $1.381 \times 10^{-6} \text{ Einstein L}^{-1} \text{ S}^{-1}$

➤ TB dye 1×10^{-4} , nanocomposite material suspended = 2 gL^{-1} , airflow rate 8.1 mL s^{-1} , Isolar = $1250 \times 100 \pm 100 \text{ Lux}$.

3.6.2 Effect of pH on photodegradation of dye

The pH of the solution has a significant impact on photocatalytic activity. The surface properties of the CeO₂ and prepared CrO₄-CeO₂ catalyst are significantly affected by the pH of the reaction medium. The effects of pH on the photocatalytic degradation of trypan blue are depicted in **Figures 3.6.2 A and B**. The figure clearly shows that the photocatalytic process is highly dependent on the pH of the dye solution [18]. The pH changes the surface properties of the nanocomposite material, causing the dye molecules to dissociate. At pH 7, per hydroxyl radicals (O₂H[•]) are formed, which results in the formation of hydrogen peroxide, which produces several hydroxyl radicals (OH[•]) [19].

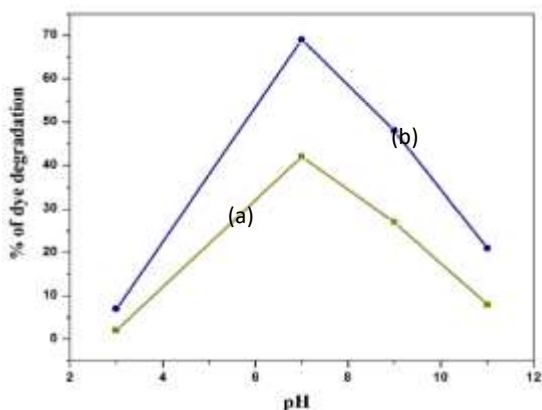


Figure 3.6.2. (A) pH study (a) CeO₂ and (b) CrO₄-CeO₂ nanocomposite material under UV

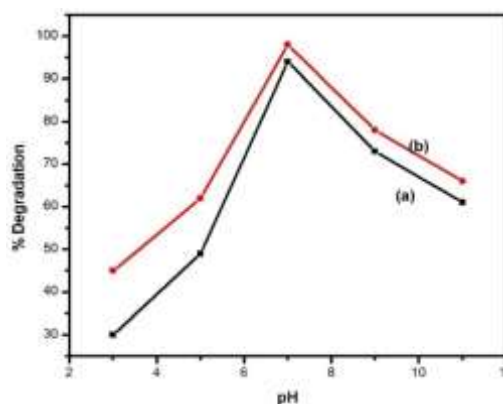


Figure 3.6.2. (B) pH study (a) CeO₂ and (b) CrO₄-CeO₂ nanocomposite material under solar-light

➤ TB dye 1×10^{-4} , nanocomposite material suspended = 2 gL^{-1} , airflow rate 8.1 mL s^{-1} , IUUV = $1.381 \times 10^{-6} \text{ Einstein L}^{-1} \text{ S}^{-1}$

➤ TB dye 1×10^{-4} , nanocomposite material suspended = 2 gL^{-1} , airflow rate 8.1 mL s^{-1} , Isolar = $1250 \times 100 \pm 100 \text{ Lux}$.



At pH 7, the highest photocatalytic degradation of CeO_2 and prepared $\text{CrO}_4\text{-CeO}_2$ is observed. It has been discovered that degradation is strongly influenced by the pH of the solution. The percentage of degradation is observed to increase up to pH =7 and then decrease. Under UV and solar light, pH 7 has superior photocatalytic activities.

3.6.3 Effect of Temperatures on photodegradation of dye

Temperature effects on catalytic reaction of $\text{CrO}_4\text{-CeO}_2$ nanocomposite material were studied from 150°C to 450°C . As the reaction temperature was raised, the equilibrium of TB removal was reached in less time, as shown in **Figures 3.6.3 A and B**. The highest percentage degradation was observed at 450°C , where 69% and 77% of TB were removed after only 60 minutes under UV and solar light, respectively. The lowest percentage degradation was observed at 300°C , where 17% and 21% of TB were removed after only 60 minutes under UV and solar light, respectively. Significantly less percentage degradation was observed at 150°C , where 9% and 11% of TB were removed after only 60 minutes under UV and solar light, respectively. At high temperatures, hydrogen peroxide easily self-decomposes, and the rate of decomposition increases with every 150°C . Superior temperatures tend to reduce the number of defects on the photocatalyst's surface area.

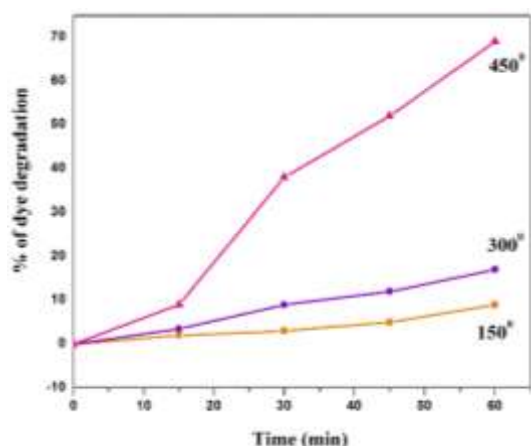


Figure 3.6.3. (A) The effects of Temperature of $\text{CrO}_4\text{-CeO}_2$ nanocomposite material nanocomposite material under UV

- TB dye 1×10^{-4} , nanocomposite material suspended = 2 gL^{-1} , airflow rate 8.1 mL s^{-1} , IUV = $1.381 \times 10^{-6} \text{ Einstein L}^{-1} \text{ S}^{-1}$

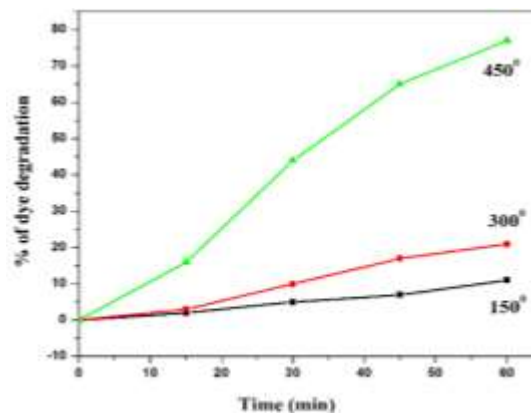


Figure 3.6.3. (B) The effects of Temperature of $\text{CrO}_4\text{-CeO}_2$ nanocomposite material nanocomposite material under solar – light

- TB dye 1×10^{-4} , nanocomposite material suspended = 2 gL^{-1} , airflow rate 8.1 mL s^{-1} , Isolar = $1250 \times 100 \pm 100 \text{ Lux}$.

3.6.4 Effect of Catalyst Loading on photodegradation of dye

One of the most important parameters in degradation studies is the amount of catalyst. To avoid the use of excess catalyst, the optimum loading for dye removal must be determined. **Figures 3.6.4 A and B** show the effect of catalyst load on the photocatalytic degradation of the dye. The catalytic (CeO_2 and $\text{CrO}_4\text{-CeO}_2$) load was varied from 0.05 to 0.1 g/50 mL to determine the optimal catalyst dosage. The ideal load was determined to be 0.08 g/50 mL. A screening effect may occur if the catalyst loading is increased beyond the optimal dosage. This effect reduces the catalyst's specific activity. Particle aggregation may reduce catalytic activity at higher catalyst dosages. Above the optimal load, slurry turbidity increases, light penetration decreases, and thus the availability of hydroxides and superoxides decreases; thus, photocatalytic activity decreases. As a result, the optimum catalyst dosage for the efficient removal of Trypan Blue (TB) dye was 0.08 g/50 mL under UV and solar light [20,21].

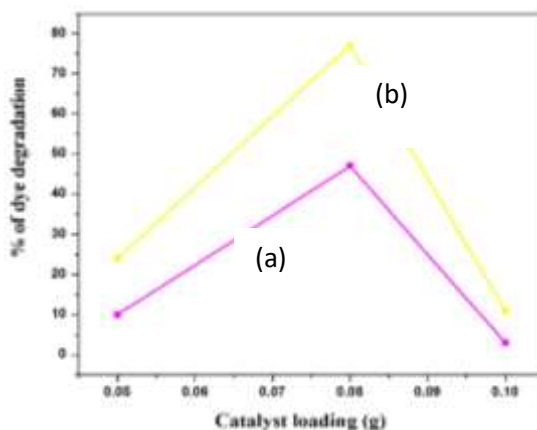
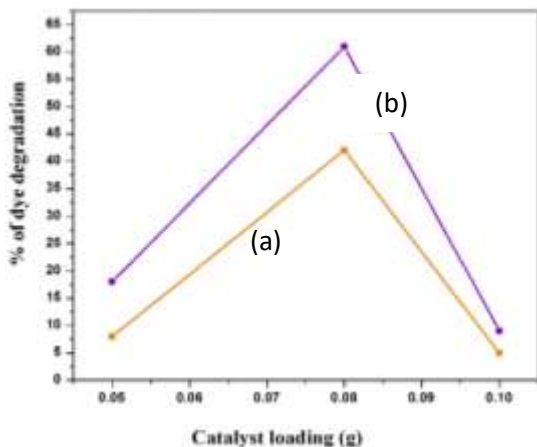


Figure 3.6.4. (A) . The effects of catalyst loading (a) CeO₂ and (b) CrO₄- CeO₂ nanocomposite material under UV irradiation

Figure 3.6.4. (B) . The effects of catalyst loading (a) CeO₂ and (b) CrO₄- CeO₂ nanocomposite material under solar-Light irradiation

➤ TB dye 1x10⁻⁴, nanocomposite material suspended=2 gL⁻¹, airflow rate 8.1 mL s⁻¹, IUUV =1.381x10⁻⁶ Einstein L⁻¹ S⁻¹

➤ TB dye 1x10⁻⁴, nanocomposite material suspended=2 gL⁻¹, airflow rate 8.1mL s⁻¹, Isolar= 1250 × 100±100 Lux.

3.6.5 Effect of Concentration on photodegradation of dye

The impact of different dye concentrations on photocatalytic degradation has been studied. The effects of dye concentration on the photocatalytic activity of CeO₂ and the prepared CrO₄-CeO₂ nanocomposite material are depicted in **Figures 3.6.5 A and B**. Trypan blue was tested at concentrations ranging from 1x10⁻⁴ to 3x10⁻⁴ M. The catalytic load was kept constant at 0.08 g and the pH was kept at 7. Under UV and solar light, the optimal dye concentration of CeO₂ and prepared CrO₄-CeO₂ nanocomposite was observed to be 1 x 10⁻⁴ M. The time required for complete dye degradation increases as the dye concentration increases. When the dye concentration is low, many active sites in the photocatalyst are vacant, and the slurry remains almost clear, allowing light to pass through. Photodegradation is aided by light penetration.

The dye molecules occupy the active sites as the dye concentration increases, and this trend continues until all of the sites are filled, which occurs at a specified optimum concentration. Beyond this concentration, the slurry becomes turbid, preventing light penetration and thus slowing degradation. A significant amount of UV and solar – light may be absorbed by the dye molecules rather than the catalyst at high concentrations, reducing catalytic efficiency [22]. Under UV and solar light, the optimum dye concentration of CeO₂ and prepared CrO₄-CeO₂ nanocomposite was observed to be 1 x 10⁻⁴ M.

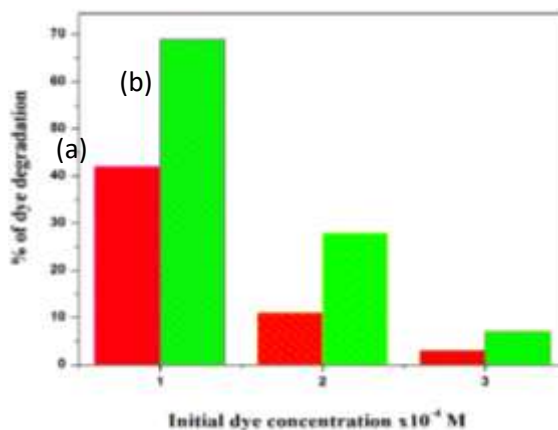
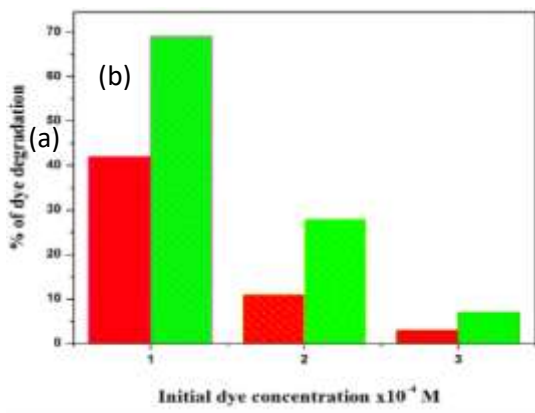


Figure 3.6.5. (A) The effects of concentrations of (a) CeO₂ and (b) CrO₄- CeO₂ nanocomposite material under UV irradiation.

Figure 3.6.5. (B) The effects of concentrations of (a) CeO₂ and (b) CrO₄- CeO₂ nanocomposite material under solar-Light irradiation.



- TB dye 1×10^{-4} , nanocomposite material suspended = 2 gL^{-1} , airflow rate 8.1 mL s^{-1} , IUUV = $1.381 \times 10^{-6} \text{ Einstein L}^{-1} \text{ S}^{-1}$
- TB dye 1×10^{-4} , nanocomposite material suspended = 2 gL^{-1} , airflow rate 8.1 mL s^{-1} , Isolar = $1250 \times 100 \pm 100 \text{ Lux}$.

3.6.6 Stability and Reusability of photocatalyst

The Stability and Reusability of the nanocomposite material were experienced by moving out the degradation with the used nanocomposite material under UV and solar-light (Figures.3.6.6 A and B). The complete degradation of TB dye in CeO_2 and prepared $\text{CrO}_4\text{-CeO}_2$ nanocomposite material under UV and solar light are 100 % & 100 %, 85 % & 85 %, 79 % & 78 %, 75 % & 78 %, 70 % & 78 % and 100 % & 100 %, 85 % & 90 %, 78 % & 84 %, 74 % & 84 % and 70 % & 84 % respectively.

Table 1.1 shows the results of five cycles of the nanocomposite material: CeO_2 and prepared $\text{CrO}_4\text{-CeO}_2$ exhibited exceptional photo stability with no significant loss of photocatalytic activity for the third to fifth cycles. The degradation efficiency of CeO_2 and the prepared $\text{CrO}_4\text{-CeO}_2$ nanocomposite material is 61 and 76% under UV light, respectively. The degradation efficiency of CeO_2 and prepared $\text{CrO}_4\text{-CeO}_2$ nanocomposite material is 78 and 84%, respectively, when exposed to solar light. These findings indicate that CeO_2 and prepared $\text{CrO}_4\text{-CeO}_2$ nanocomposite material remain effective and reusable when exposed to solar light. The final result shows that solar-light irradiation has higher photocatalytic activity than UV-light irradiation.

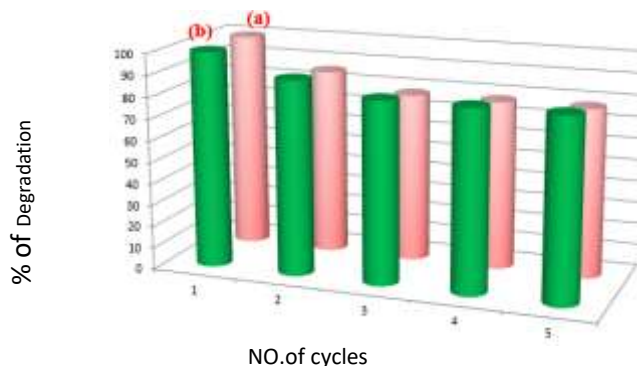
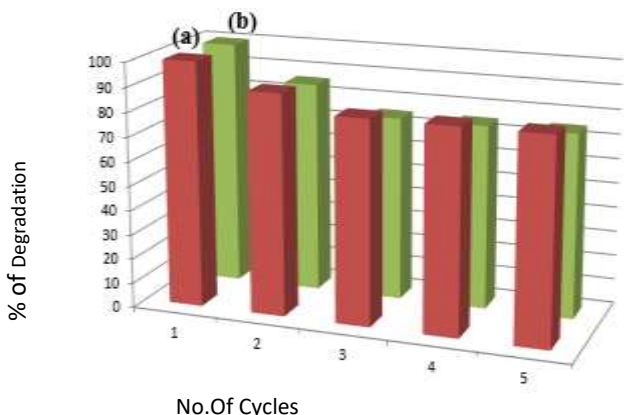


Figure 3.6.6 (A) Stability and Reusability on TB dye degradation; (a) CeO_2 and (b) $\text{CrO}_4\text{-CeO}_2$ nanocomposite material under UV-light irradiation

- TB dye 1×10^{-4} , nanocomposite material suspended = 2 gL^{-1} , airflow rate 8.1 mL s^{-1} , IUUV = $1.381 \times 10^{-6} \text{ Einstein L}^{-1} \text{ S}^{-1}$

Figure 3.6.6 (B) Stability and Reusability on TB dye degradation; (a) CeO_2 and (b) $\text{CrO}_4\text{-CeO}_2$ nanocomposite material under Solar-light irradiation

- TB dye 1×10^{-4} , nanocomposite material suspended = 2 gL^{-1} , airflow rate 8.1 mL s^{-1} , Isolar = $1250 \times 100 \pm 100 \text{ Lux}$.

Table 1.1 Nano Catalyst Reusability under UV & Solar light

No of cycles	Percentage of TB removal on CeO_2		Percentage of TB removal on $\text{CrO}_4\text{-CeO}_2$	
	UV	Solar	UV	Solar
1	100	100	100	100
2	85	85	85	90
3	79	78	78	84
4	75	78	74	84
5	70	78	70	84

4. Mineralization Study

4.1 Chemical Oxygen Demand Analysis (COD)

The chemical oxygen demand (COD) analysis is an important indicator of organic pollution in water. The COD for the degradation of Trypan Blue (TB) dye on prepared $\text{CrO}_4\text{-CeO}_2$ nanocomposite material loading amount of 0.08 gram on dye initial concentration $1 \times 10^{-4} \text{ M}$ suspension for 40 mL of PH 7 solution and air passing with UV 365nm was measured. The chemical oxygen demand test is a popular method for determining the organic strength of wastewater. The waste can be measured in terms of the total amount of oxygen required for the oxidation of organic matter to CO_2 and water. The dye solution's COD before and after treatment was calculated. The

reduction in COD values of the treated dye solution indicates dye molecule mineralization as well as color removal. The COD values of blank and treated dye solutions are shown in **Table.1.2**.

Table .1.2 Percentage of chemical oxygen demand analysis of Trypan Blue (TB)

Sl. NO.	Time (Min)	COD Values		% of degradation of Trypan Blue with CrO ₄ -TiO ₂
		Initial COD (mg/50ml)	Final COD (mg/50ml)	
1	60	4.5	1	77

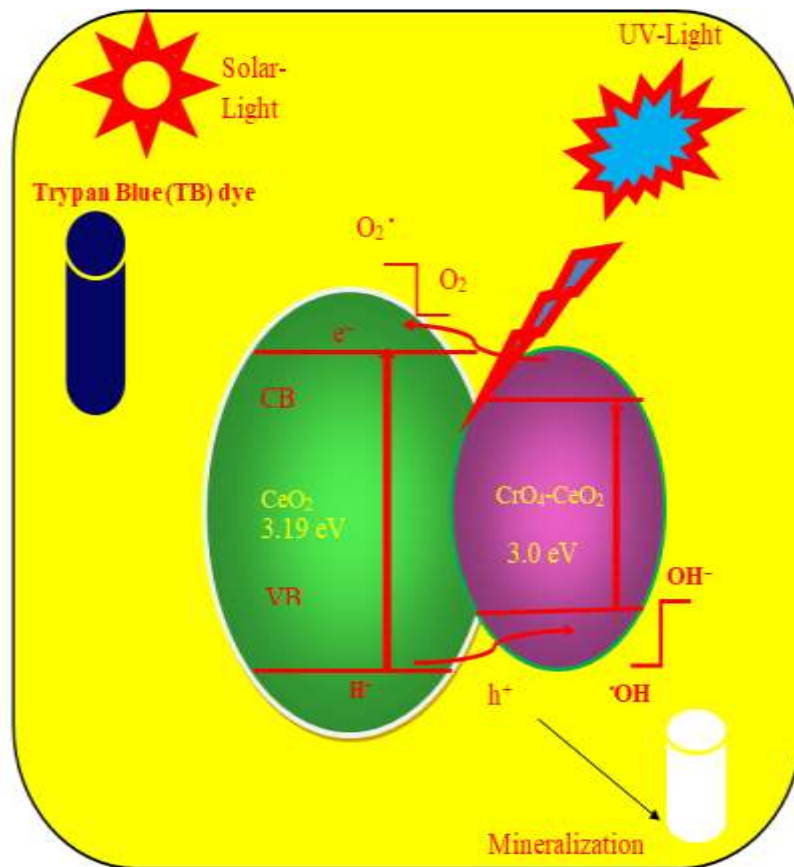
4.2 Mechanism of Degradation

From the photocatalytic mechanism results, a process based on photo-carrier transfer is discovered. With 365 nm light, CeO₂ is excited upon irradiation. The transfer of the photoexcited electron from the surface of CeO₂ to CrO₄ nanoflower occurs in the case of CrO₄ altered CeO₂ due to greater positive conduction band potential. The charge carriers are thus effectively separated. Electrons stored on the nanocomposite material conduction band are absorbed by adsorbed O₂ molecules. The result is super oxide radicals (O₂⁻) being formed. TB dye molecules are decomposed by these superoxide radicals and hydroxide radicals formed by holes [23,24]. It is shown in **Scheme 1.1**.

5 ELECTRO CATALYTIC APPLICATION

5.1 Dye Sensitized Solar Cells Analysis

The **Figures 5.1. a** and **b** show that the fabrication activity of photo current-voltage (I-V) in the sensitized solar cells (DSSCs) dye as photoelectrode, as photo electrodes are coated on the fluorine-doped tin oxide (FTO-plate) glass substrate, prepared CeO₂ and prepared CrO₄-CeO₂ nanocomposite material act as photoelectrode. The routine solar cell is fabricated with Prepared CeO₂ and prepared CrO₄-CeO₂ nanocomposite material with Ruthenium dye (535-bisTBA, N719).



Scheme. 1.1. Schematic representation for the photodegradation holes and electrons in the Nanocomposite material under Solar and UV- light for successive mineralization of TB dye.



From the data, it is clear that (N719) on prepared CrO₄-CeO₂ nanocomposite material-based cell gives the mainly brilliant activity with the use of dye as sensitizer reunite the maximum value of short-circuit current density, J_{sc} (3.5 mA/cm²) than CeO₂ (3.25 mA/cm²), open-circuit voltage, V_{oc} (500 mV), fill-factor, FF (0.94 and efficiency, η (1.7 %). The outcome indicates successful electron transfer of prepared CrO₄-CeO₂ nanocomposite material and keeps back the recombination of the photo generated charge carrier, thus increasing the short circuit current and electron transfer [25].

Photocurrent-photovoltage (I-V) measurement the overall conversion efficiency of the dye-sensitized solar cell calculated by

(I_{sc}) = Photocurrent density measured at short circuit current

(V_{oc}) = photovoltage open-circuit

(FF) = filling factor of the cell and

(P_{in}) = input optical power the formula known as

Efficiency = $[I_{sc} \times V_{oc} \times FF / P_{in}] \times 100\%$

Where P is the input optical power, and I_{sc}, V_{oc}, are determined from the photocurrent-photovoltage curve of the cell [26-30].

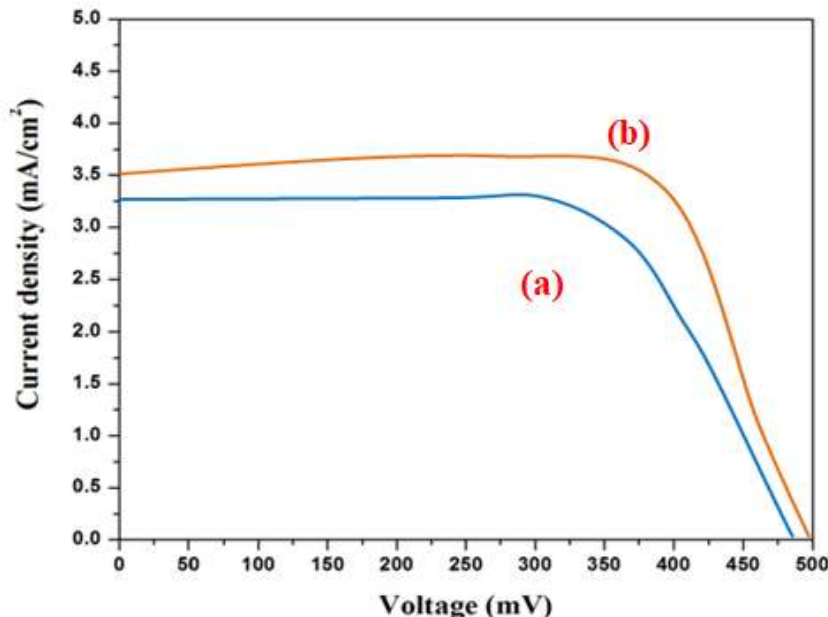


Figure. 5.1 Current density–voltage (I–V) curves for the DSSC’s fabricated from (a) CeO₂ and (b) CrO₄- CeO₂ nanocomposite material

6.CONCLUSION

The prepared CrO₄-CeO₂ nanocomposite material was synthesized using a co-precipitation method and was characterized by HR-SEM and HR-TM analysis for spherical morphology structure, with X-ray (EDX) analysis confirming the presence of Cr, Ce, and O in the nanocomposite material. XRD analysis revealed that the average crystalline size of CeO₂ and prepared CrO₄-CeO₂ is 29 nm and 23.2 nm, respectively. The decrease in PL (CrO₄-CeO₂) intensity results in CeO₂'s high photocatalytic activity. The UV-Vis DRS spectrum had low bandgap energy, allowing it to function as an efficient photocatalyst and to be used in DSSCS applications. The photocatalytic application of TB dye under Solar-Light has a highly photocatalytic application that was done with UV-Light irradiation for 60 minutes. The prepared nanomaterial was found to be stable and reusable after an achievable mechanism was proposed and the nanomaterial was discussed extensively. According to the electrochemical analysis results, the prepared CrO₄-CeO₂ nanocomposite material is effective in electron transfer and inhibits photogenerated charge carrier recombination, which improves electron transfer and increases short circuit current.

Credit Authorship Contribution Statement

K. Subashri: Writing - original draft, Writing - review & editing, Conceptualization, Data curation, Methodology.



Declaration of Competing Interest

The authors declare that they have no known competing financial interests or personal relationships that could have appeared to influence the work reported in this paper.

REFERENCE

1. Thammadihalli Nanjundaiah Ravishankar, Thippeswamy Ramakrishnappa, Ganganagappa Nagaraju and Hanumanaika Rajanaika, *Chemistry open* 4, 146-154, DOI: 10.1002/open.201402046, 2015.
2. T. Masui, H. Hirai, N. Imanaka, G. Adachi, T. Sakata, H. Mori, *J. Matter.Sci.Lett*, 21, 489-491, 2002.
3. Kumar, S. Babu, A.S. Karakoti, A. Shulte, S. Seal, *Langmuir* 25 10998-11007, 2009.
4. D. Damatov, J.M. Mayer, *Chem. Commun.* 52 10281-10284, 2016.
5. D. Saravanakumar, H. Abou Oualis, Y. Brahmi, A. Ayeshamariam, M. Karunanaiathy, A. Mohamed Saleem, K. Kaviyarasu, S. Sivaranjini, M. Jayachandran, *Open nano*, 4 100025, 2019.
6. C. Zhang, X. Zhang, Y. Wang, S. Xie, Y. Liu, X. Lu, Y. Tong, *New J Chem.* 38 2581-2586, 2014.
7. E. Kumar, P. Selvarajan, D. Muthuraj "synthesis and characterization of CeO₂ nanoparticles by solvothermal Route" *material Research September* 3,2012.
8. R.K.Hailstone , A.G.Difrancesco , K.J. Reed "synthesis and characterization of CeO₂ nanoparticles" *Microsc microanal* 15 (suppl2), doi :10.1017/S1431927609096548, 2009.
9. R. Thammadihalli, *Chemistry open* 4, 146, DOI: 10.1002/open.201402046, 2015.
10. GG.Hu et.al., ZL. *Direct synthesis and structure characterization of ultrafine CeO₂ nanoparticles.Nanotechnology*.7,897.http://dx.doi.org/10.1088%2F0957-4484%2F17%2F24%2F013, 2006.
11. R.C.Deus et.al., *Simoes Materials research bulletin* 70, 416, DOI: 10/1016/J.Materresbull.2015. 05. 006, 2015.
12. Y.W. Zhang et.al., *Fe doped CeO₂ nanoparticles*, *J. Phys. Chem. B* 107, 10159,.D. P. Jaihindh, C. C. Chen, Y. P. Fu, *RSC Adv.* 2018, 8, 6488, 2003.
13. D. Malwal, P. Gopinath, *Catal. Sci. Technol.* 6, 4458, 2016.
14. D.P. Jaihindh et.al., *RSC Adv.* 8, 6488, 2018.
15. S. Rasalingam et.al., *Applied Catalysis B: Environmental*, 148, 394, 2014.
16. H.Q.Cao et.al., *Adv. Funct. Mater.* 14, 243, 2004.
17. M. Shivaram et.al., *Mater. Res. Bull.* 48, 67, 2013.
18. W.S. Dong et.al., *Colloid Interface Sci.* 333, 734, 2009.
19. J. Zhang et.al., *RSC Adv.* 6, 1399, 2016.
20. T. K. Ghorai, *Open. J. Phys. Chem.* 1, 28
21. S.Sakthivel et.al., *Chem. Int. Ed.*, 42, 4908, 2003.
22. C.Guillard et.al., *JM, Appl. Catal., B*, 46, 319, 2003.
23. V.L. Chandraboss et.al., *Mater. Res. Bull.*, 48, 3707-3712, 2013.
24. B. Subash et.al., *Catal. Sci. Technol.*, 2, 2319, 2012.
25. G. L. J. Zhao, *New J. Chem.*, 24, 411, 2000.
26. X. Ni et.al., *Colloids Surf. A* 567, 161, 2019.
27. R. Verma, S. K. Samdarshi, *J. Phys. Chem. C* 120, 22281, 2016.
28. G. Gopakumar, V. Shantikumar Nair and M. Shanmugam, *Nanoscale, Advances*, DOI: 10.1039/d0na00158a, 2020.
29. M. Gratzel, "Dye-Sensitized Solid-State Heterojunction Solar Cells", *MRS Bulletin*, 30, 23, 2005.
30. TN. Murakami, M.Gratzel , *Inorg Chim Acta*, 361,572, 2008.